Biological Disposition and Imaging of a Radioiodinated Alkylphosphocholine in Two Rodent Models of Breast Cancer

Mark A. Rampy, Raya S. Brown, Anatoly N. Pinchuk, Jamey P. Weichert, R.W. Scott Skinner, Susan J. Fisher, Richard L. Wahl, Milton D. Gross, Stephen P. Ethier and Raymond E. Counsell

Departments of Pharmacology, Internal Medicine, Nuclear Medicine, Radiology, and Radiation Oncology, The University of Michigan Medical School; and Nuclear Medicine Service, Department of Veteran's Affairs, Ann Arbor, Michigan

Iodine-125-12-[*m*-iodophenyl]-dodecylphosphocholine (NM-324) has been shown to accumulate in a variety of animal tumor models. Moreover, preliminary pharmacokinetic studies with NM-324 are being conducted in cancer patients. The present study was undertaken to examine the potential application of NM-324 as a breast tumor-imaging agent. **Methods:** Two animal models of breast cancer were utilized: namely, syngenic inbred Lewis male rats bearing the rat mammary tumor (RMT) and athymic mice with HT-39 human tumor xenografts. After i.v. administration of NM-324, the tissue distribution of radioactivity was determined at various time points. Gamma camera scintigrams were also acquired to confirm the biodistribution results. Macro- and microautoradiography were used to analyze cellular distribution of radioactivity in tumors. **Results:** In the rat mammary tumor model, levels of radioactivity in the tumor reached a maximum at 24 hr after i.v. administration (1.65% ID/g, tumor-to-blood 6.4). These tumors could be visualized by gamma camera scintigraphy as early as 1 hour after administration. In the nude mouse model, levels of radioactivity in tumor reached a maximum at 48 hr after i.v. administration (4.96 %ID/g, tumor-to-blood 5.5). Tissues expected to interfere with the resolution of breast lesions such as fat, heart, lung and muscle displayed much lower concentrations of the radioactivity. Gamma camera scintigraphy confirmed the results observed from biodistribution experiments. Lipid extraction of the tumors and major organs in both animal models showed the sole presence of unchanged NM-324. Microautoradiographic analysis of slices of rat mammary and HT-39 tumors provided additional information regarding the intratumoral distribution of radioactivity. **Conclusion:** The ability of radioiodinated phospholipid analogs to accumulate in breast tumors reinforces the need for further investigation of this type of radiopharmaceutical as tumor imaging agents.

Key Words: radioiodinated phospholipid ethers; tumor localization; breast cancer

J Nucl Med 1996; 37:1540–1545

Early detection of breast cancer remains a major goal of nuclear medicine studies. Approaches in the design of radiopharmaceuticals to accomplish this goal have included specific monoclonal antibodies (*1–3*), steroid hormone receptor-mediated processes (*4–7*) and metabolic trapping with agents such as [^{18}F]fluorodeoxyglucose (*8–10*).

Our own strategy has taken advantage of a unique biochemical characteristic of malignant cells which was observed in tumor tissue by Snyder et al. (*11–13*) in the late 1960s. They discovered that a variety of both animal and human tumors contained much larger quantities of naturally occurring ether

lipids in the cell membranes relative to corresponding normal tissues. We have previously synthesized a variety of radioiodinated phospholipid ether (PLE) analogs and demonstrated them to be selectively retained by a variety of rodent and human tumors (*14–17*). It was possible to obtain images of these tumors in rabbits, rats and mice using gamma camera scintigraphy. Based on these and other preliminary results, the use of one of these radioiodinated analogs, 12-(*m*-iodophenyl)dodecyl phosphocholine (NM-324) is currently undergoing clinical evaluation as a radiopharmaceutical in cancer patients.

In the present study, we sought to evaluate NM-324 as a potential agent for imaging breast tumors. Two animal models of breast cancer were utilized in this study. Biodistribution and tumor uptake were studied in syngeneic inbred Lewis rats bearing the rat mammary tumor (RMT) (*18–20*) and in athymic nude mice with HT-39 human tumor xenografts (*21–23*). Both macro and microautoradiography were performed on kidney, liver, and tumor tissue isolated from Lewis rats and athymic mice. In addition, gamma camera scintigrams were acquired at various time points to determine the suitability of NM-324 as a potential imaging agent.

MATERIALS AND METHODS

Preparation of Iodine-125-NM324

Radioiodinated NM324 was made via isotope exchange in pivalic acid (*24*). Briefly, unlabeled 12-(*m*-iodophenyl)dodecyl-phosphocholine (0.5 mg) (*16*) was placed in a 300-μl V-vial (Wheaton, Millville, NJ) fitted with teflon faced seal and screw cap. Absolute ethanol (20 μl) was added via a microliter syringe followed by aqueous Na^{125}I (0.5–3.0 mCi, 2–10 μl) no-carrier-added in reductant-free 0.1 N NaOH from Amersham Radiochemicals). The vial was gently swirled to dissolve the contents and ensure homogeneity. Inlet and outlet cannuli were inserted and a gentle stream of nitrogen was applied to remove the solvents. Two successive in-line charcoal traps were placed on the outlet side in order to trap any volatile radioiodine present in the reaction vial. Once dry, solid pivalic acid (10 mg), previously dried by azeotropic removal of water with toluene and distilled under nitrogen, was added. The vial was sealed and heated at 160°C in a preheated single well aluminum heating block containing 1 cm of sand in the bottom of the well. After 1 hr, the reaction vial was removed from the heating block and allowed to cool to room temperature. Absolute ethanol (70 μl) was added through a micro syringe followed by gentle agitation and subsequent removal of a TLC sample (1–2 μl). The entire contents of the reaction vial were then injected directly onto a silica gel HPLC column eluted with hexane/isopropanol/water (40:52:8) at 0.8 ml/min.). Peaks were analyzed by both UV (230 and 254 nm) and radiodetection. After pooling appropriate fractions, the radiochemical purity of the final

product was monitored by TLC (gamma and UV detection) and by HPLC (UV at 230/254 nm and radiochemical detector). Fractions were combined and the solvent was removed with a gentle stream of nitrogen. HPLC analysis of the final compound confirmed both chemical (UV at 230/254 nm) and radiochemical (radioactivity) purity. Specific activity of injected compounds ranged from 0.56–11.7 Ci/mmole as determined by HPLC comparison with known standards. Labelling efficiency determined by electronic integration of radio-TLC traces of the crude reaction mixtures ranged from 40% to 71%. After HPLC purification, from 38% to 58% of the initial radioactivity was isolated as NM324 and in all cases, radiochemical purity of final compound exceeded 95%.

Cell Lines and Culture Conditions

Frozen rat mammary tumor cells (1–9 RMT transplant generation 4) were thawed for implantation into the Lewis rats. These cells were provided by one of the authors (S.E.). HT-39 breast cancer cells were grown in monolayer culture in Dulbecco's Modified Eagle's Medium (DMEM) containing 10% fetal bovine sera, 100 U/ml penicillin and 100 μg/ml streptomycin. HT-39 estrogen-independent human breast tumor cells were provided by Dr. Robert Simpson. Stock cultures were maintained in 162 cm^2 flasks and incubated in humidified atmosphere of 95% air and 5% CO_2. Populations were subcultured every 5–7 days. Exponentially growing cells were used in all experiments.

Animal Models

Female inbred Lewis rats, 200–250 g were housed in a temperature and light-controlled room and had free access to food and water. RMT cells were implanted (10^6 cells/animal) in the interscapular fat pads of five syngeneic female Lewis rats while under ether anesthesia as previously described (18–20). Tumors appeared in 100% of the host animals within 4–6 wk. Three of these animals were subjected to gamma camera scintigraphy. Two of the rats were killed and the tumors were aseptically removed, minced and transplanted into 28 rats as previously described (18–20). The 28 rats were then used 4–6 wk later for biodistribution analysis and gamma camera scintigraphy. Tumors appeared in 100% of the host animals.

CD-1 *nu/nu* athymic mice (6–8 wk old) were housed in sterile laminar flow rooms with free access to autoclaved chow and water. HT-39 cells (10^6 cells/animal) were suspended in sterile phosphate buffered saline (200 μl) and implanted subcutaneously in the shoulder region of the mice using a 23-gauge needle as previously described (21–23). Tumors appeared 4–6 wk later. All procedures using animals conformed strictly to the guidelines set forth by the University of Michigan Unit of Laboratory Animal Medicine which reviewed and approved the experimental protocol.

Biodistribution Studies

The radiolabeled compound was dissolved in absolute ethanol (50–500 μl) and Tween-20 (0.1 ml/mg of compound) was added to the solution. Ethanol was removed by evaporation under a stream of nitrogen. Physiological saline was added, to give a 2–3% Tween-20 solution which was subsequently mixed by vortex. The solubilized radiolabeled compound was administered *via* tail vein. Anesthetized tumor bearing rats received 5–10 μCi, 0.5 ml and athymic mice received 5–10 μCi in 0.1 ml. At various times postinjection (n = 3 per time point), animals were killed by exsanguination while under ether anesthesia. Blood samples were collected through cardiac puncture and selected tissues (liver, kidney, etc) were removed, trimmed, blotted to remove excess blood and weighed. Twenty-one tumored rats and 21 tumored mice were studied. Large organs were thoroughly minced with scissors to obtain random representative tissue samples. Tissue samples from the various organs (n = 2 per tissue) were weighed and

placed in gelatin capsules and counted in a Searle-1185 well scintillation counter (88% efficiency). The concentration of radioactivity in each tissue was expressed as a percentage of injected dose per gram of tissue (%ID/g) or percent injected dose per whole organ. Tumor-to-nontarget tissue ratios were calculated based on the percentage of injected dose per gram of tissue data.

Lipid Extraction

Samples of liver and tumor were homogenized in $CHCl_3$:MeOH by the method of Folch et al. (25). Briefly, 0.2 g tissue and 0.3 ml water were homogenized in three washes of 3 ml each of $CHCl_3$:MeOH (2:1) and the resulting homogenate filtered. The filter papers were air-dried and assayed for radioactivity. The filtrate was adjusted to 10 ml with $CHCl_3$:MeOH, and an additional 2 ml H_2O was added and centrifuged for 10 min at 800 g. The aqueous and organic phases were separated and analyzed by thin-layer chromatography as previously described (17).

Preparation of Tissues for Frozen Sections

The kidneys, liver, and rat mammary tumor were removed from one Lewis rat 24 hr after i.v. injection of 100 μCi of NM-324. Kidneys, livers and HT-39 tumors were excised from two athymic mice 48 hours after i.v. injection of 50 μCi of NM-324. An additional mouse injected with vehicle only served as a control. The time points were selected to coincide with the highest %ID/g levels of radioactivity in the tumor for each model. Each of the excised tissues were divided into two equal parts, one to be used for autoradiography and the other for conventional histology. Tissue samples to be used for autoradiography were frozen in 2-methyl-butane (isopentane) cooled in liquid nitrogen and stored at $-70°C$ until used. The second part was fixed overnight in buffered formalin and processed for conventional histology.

Sets of three consecutive frozen sections, 16-μm thick for macroautoradiography and 6-μm thick for microautoradiography, were sectioned at intervals of 800 μm through the frozen part of the tumors, and collected on frozen slides and quickly dried as previously described (26).

Autoradiography

Macroautoradiography. Slides with dried 16-μm thick sections were placed in x-ray cassettes and the sections were exposed to films at room temperature for 18 or 36 hr, depending on the activity in the tissues.

Microautoradiography. Slides with dried 6-μm thick sections were dipped in nuclear emulsion diluted 1:1 with distilled deionized water at 42°C. The slides were dried at room temperature and exposed at 4°C for 7–28 days. The slides were then developed in Kodak D-19 and counter stained with Lee's stain as was previously described (27). Grains were counted over areas of viable looking tumor cells and over necrotic areas 3 (20 × 40 μm) areas.

Gamma Camera Scintigraphy

Whole-body scanning of the animals was performed using a camera equipped with a high-sensitivity collimator using a photo-peak window optimized for ^{125}I. Image acquisition and storage was accomplished with a computer connected to a larger unit. Rats (n = 3) were sedated with a premixed solution 87 mg/kg ketamine and 13 mg/kg xylazine i.m. Mice (n = 2) were sedated by i.m. injection using a premixed solution of 7 mg xylazine and 36 mg ketamine in dose of 70–80 mg/kg based on ketamine content. The animals were placed on their right sides on the camera and scanned for 20 min to generate a lateral image. Images were accumulated at various time points after tail-vein administration of radiolabeled compound (65–120 μCi, 0.5–1.0 ml/rats, 30–40 μCi, 0.1 ml/mouse).
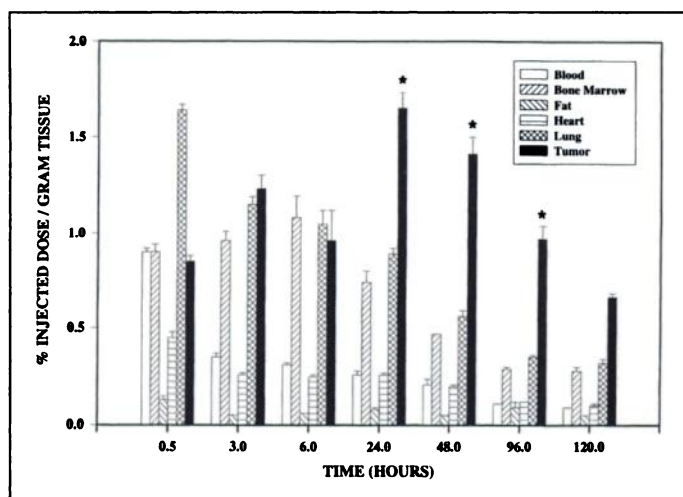
FIGURE 1. Biodistribution of NM-324 in rat mammary tumor-bearing rats. Liver reaches a maximum of 5.89 ± 0.44 %ID/g at 3 hr. *p < 0.05.
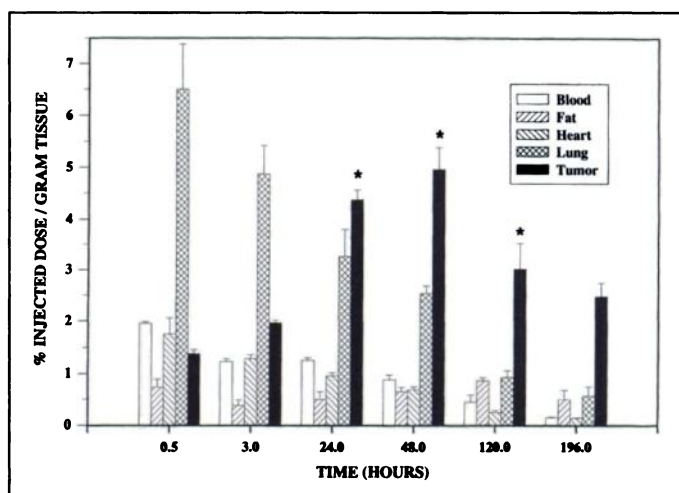

FIGURE 2. Biodistribution of NM-324 in HT-39 tumor-bearing athymic mice. Liver reaches a maximum of 39.12 ± 2.17 %ID/g at 0.5 hr. *p < 0.05.

RESULTS

The results of the biodistribution analysis of NM-324 in rats bearing the RMT tumor are presented in Figure 1 and Table 1. Rat mammary tumor weights ranged from 3.1 to 8.9 g. Radioactivity uptake in the tumor continued to increase with time and reached a maximum level of 1.65 %ID/g by 24 hr as opposed to a decrease in blood levels from 0.90 %ID/g to 0.26 %ID/g (Fig. 1). Figure 1 presents the levels of radioactivity in nontarget tissues that would provide the major sources of background activity when imaging the breast. Between 24 and 120 hr, the levels of radioactivity declined in both blood and tumor to 0.09 and 0.66 %ID/g, respectively. With the exception of fat, the tumor-to-normal tissue ratios reached a maximum at 96 hr after administration when the tumor-to-blood ratio was 8.6 (Table 1).

The results for the biodistribution analysis of NM-324 in the athymic mice bearing the HT-39 tumors are presented in Figure 2 and Table 2. The HT-39 tumors ranged in weight from 0.4 to 1.3 g. Levels of radioactivity in the tumor gradually increased to a maximum of 4.96 %ID/g at 48 hr as compared to blood levels of 0.89 %ID/g. Levels of radioactivity in relevant nontarget tissues reached the maximum at earlier time points (Figure 2). Duodenum, kidney and liver had levels of radioactivity that exceeded those of the tumor at time points up through 120 hr. This is illustrated in Table 2 which lists the tumor-to-normal

tissue ratios for the HT-39 tumor-bearing mice. In all cases, tumor-to-nontarget ratios peaked at 196 hr and provided a tumor-to-blood ratio of 16.9, and a tumor-to-muscle ratio of 19.1. By 196 hr, the tumor-to-nontarget ratio for all tissues surveyed was greater than one and revealed that normal tissues could clear the radioactivity more rapidly than tumor.

Radio-TLC analysis of lipid extracts of liver and tumor samples taken from RMT-bearing Lewis at 24 and 120 hr and HT-39 tumor-bearing mice at 48 and 196 hr after administration revealed the presence of intact parent compound (data not shown).

In macroautoradiograms of HT-39 tumors, most of the radioactivity was retained in the outer regions of the tumors with very little activity in the center (data not shown). In RMT tumors, heterogeneous levels of radioactivity were seen throughout the tumor. The activity was seen mainly in the parenchyma with very little activity in the connective tissue stroma (data not shown).

Histologically, the outer region of the HT-39 tumors consisted of large viable cells and the inner, somewhat liquefied center that was mostly necrotic. The viable cells were arranged in sheets or cords and did not form any distinct structure (Fig. 3A, B). Most of the silver grains seen in the microautoradiograms were located in the outer regions (Fig. 3A) and relatively few grains were located in the necrotic center of the tumor (Fig. 3B). The numbers of silver grains counted per cell in areas of

TABLE 1
Tumor-to-Normal Tissue Ratios* for Rat Mammary
Tumor-Bearing Rats

Organ	24 hr	48 hr	96 hr	120 hr
Adrenal	4.12	4.40	5.36	3.91
Blood	6.44	6.61	8.62	6.71
Bone Marrow	2.23	2.99	3.33	2.37
Duodenum	0.69	0.64	1.13	0.57
Fat	20.64	28.14	10.73	13.28
Heart	6.45	6.97	8.40	6.57
Kidney	0.36	0.40	0.44	0.34
Liver	0.57	0.59	0.74	0.61
Lung	1.85	2.54	2.74	2.06
Muscle	21.44	18.51	20.13	15.44
Ovary	4.59	4.40	5.37	4.15
Plasma	5.79	5.65	7.67	5.98
Spleen	2.46	3.11	3.45	2.60

*% dose/g tumor/% dose/g normal tissue.

TABLE 2
Tumor-to-Normal Tissue Ratios* for HT-39 Tumor-Bearing Mice

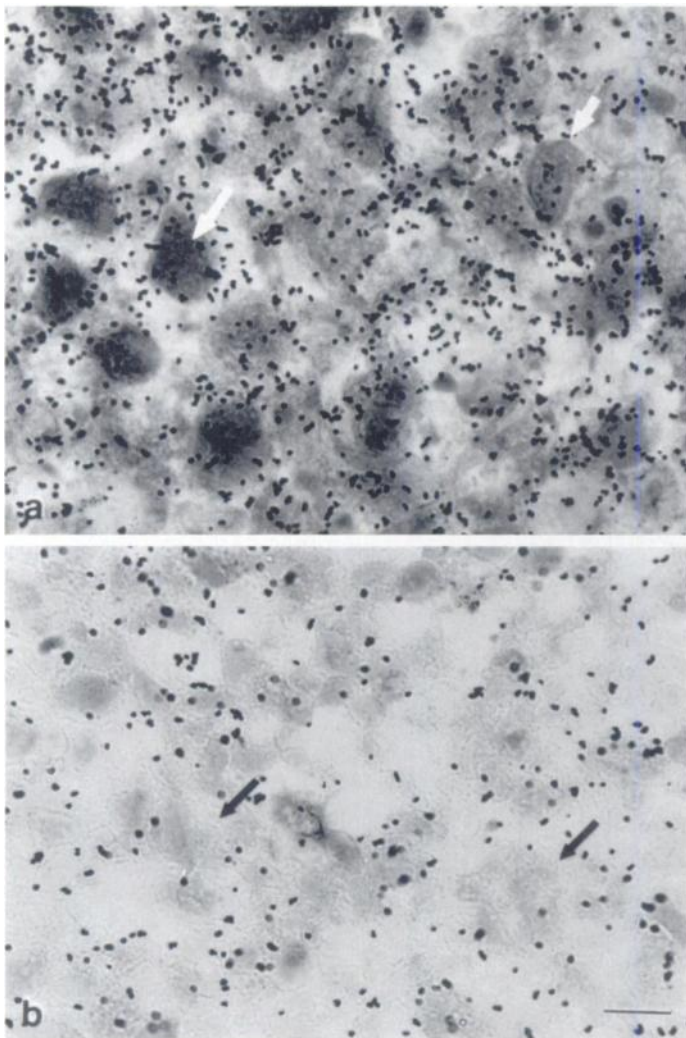| Organ	24 hr	48 hr	120 hr	196 hr
Adrenal	2.41	2.84	3.64	3.66
Blood	3.50	5.55	6.70	16.93
Duodenum	0.18	0.31	0.90	2.66
Fat	8.71	7.60	3.50	4.96
Heart	4.57	7.18	12.32	17.61
Kidney	0.29	0.51	0.87	—
Liver	0.26	0.44	0.74	1.49
Lung	1.22	1.96	3.23	4.36
Muscle	11.96	13.24	15.59	19.12
Ovary	1.47	2.67	4.29	4.73
Plasma	4.52	5.23	12.40	9.16
Spleen	1.93	3.20	5.32	8.54

*% dose/g tumor/% dose/g normal tissue.

FIGURE 3. Microautoradiographs of sections from HT-39 xenograft grown in an athymic mouse. Sections (6-μm) of tumor were processed as described in Materials and Methods. Mag. 800×; Bar = 10 μm. (A) Outer region of tumor. Silver grains are seen in viable tumor cells with heterochromatic nuclei (white arrows). (B) Region from the center of the same tumor. Few silver grains are seen in this area which consists of cell 'ghosts' (black arrows).

FIGURE 4. Microautoradiographs of sections from rat tumors. Sections (6-μm) of the tumor were processed as described in Materials and Methods. (A) Region from the tumor. Larger number of silver grains are seen in tumor cells. Fewer silver grains are seen in large 'empty' lumen (ll) as compared to a small lumen containing necrotic cells (sl). Note clusters of grains along the cell membrane facing the lumens (arrow heads). Mag. 500×; Bar = 20 μm. (B) In some cells, silver grains are located on or circling the cell nucleus (white arrow) and sometimes the cell membrane (white trimmed arrowheads). Mag. 800×; Bar = 10 μm.

viable cells 26.4 ± 3.2 was significantly higher than the numbers counted in areas of necrosis 10.17 ± 0.95.

The RMT tumor was mostly glandular in structure and the mostly microscopical necrotic foci contained large number of infiltrating inflammatory cells. Larger numbers of silver grains were observed in areas of viable tumor cells than in 'empty' lumens or in the connective tissue stroma (Fig. 4A, B) and high clusters of silver grains were observed along the cell membrane facing the lumen (Fig. 4A). In contrast to the HT-39 xenografts, the small necrotic foci retained in many cases as much activity as adjacent areas of viable cells (Fig. 4A).

The patterns of the disposition of radioactivity in the kidneys, livers and tumors were ascertained by macro- and microauto-radiographic analysis. Radioactivity appeared to be evenly distributed in autoradiograms of liver samples from both animals (data not shown) but the levels of radioactivity retention between the various histological regions of the kidneys differed. In the kidneys of both animals, the highest levels of radioactivity were observed in the renal cortex while distinctively lower levels were seen in the other areas and essentially no activity was observed in the calyx and renal pelvis (data not shown).
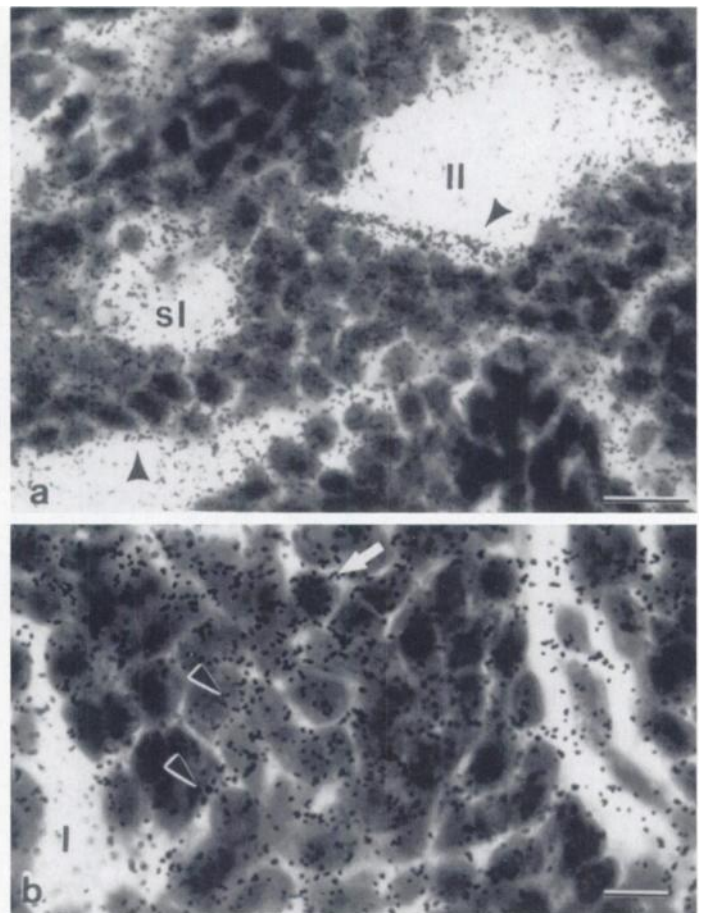
Scintigraphic images of rat mammary tumor-bearing rats

were obtained at 1, 3, 6, 24 hr and then at 24-hr intervals up to 120 hr after administration. As shown in Figure 5, NM-324 afforded visualization of the tumor as early as 1 hr after i.v. administration. By 24 hr, the whole-body image displayed high background activity, primarily located in the abdominal area which partially cleared by 120 hr. The bulk of this abdominal activity was associated with liver, kidney and the gastrointestinal tract, as confirmed by the biodistribution studies. However, the tumor was clearly discernible at all time points.

Gamma camera scintigraphy was also performed on athymic mice at 6, 24, 48, 72, 96, 120, 168 and 196 hr after administration. Tumors were readily visible as early as 6 hr after administration. Similar to the rat, whole-body scans at 48 and 196 hr displayed high levels of activity in the abdominal regions of the mouse and tended to obscure precise delineation of the tumor (data not shown).

DISCUSSION

The potential of a radioiodinated phospholipid ether analog for breast tumor imaging was investigated in this preliminary study. It was found that tumors retained more radioactive NM-324 than adjacent nontarget organs. The tissue distribution studies in Lewis rats bearing the rat mammary tumor revealed that levels of radioactivity reached a maximum of 1.65 %ID/g in the tumor at 24 hr after i.v. injection of NM-324. Total tumor
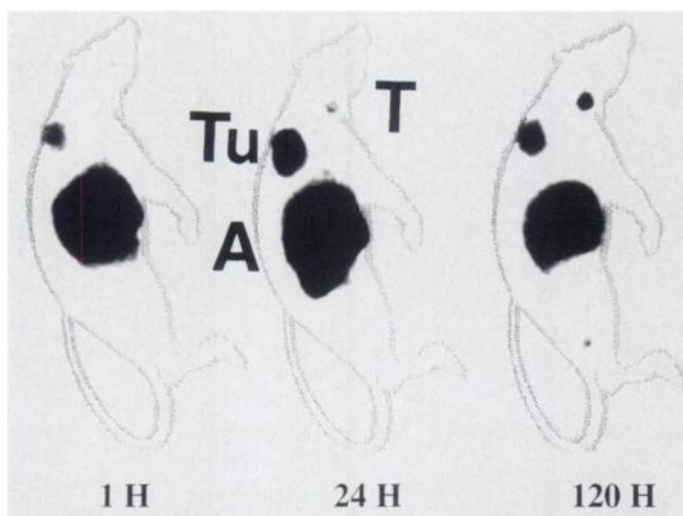
FIGURE 5. Gamma camera images of NM-324 in a female Lewis rat (lateral view) with a rat mammary tumor after i.v. administration of 140 μCi ^{125}I-NM-324 A = activity associated with gastrointestinal tract, including kidneys; T = thyroid; TU = tumor).

uptake at 24 hr after injection amounted to approximately 5.2% of the injected dose. Similar results were obtained in our laboratory with NM-324 in Sprague Dawley rats with the Walker 256 carcinosarcoma implanted i.m. in the leg (16). The levels of radioactivity in the tumors at 24 hr after i.v. injection was approximately 1.5 %ID/g. The similarity in the levels of NM-324 in the relatively slow growing RMT and the fast growing Walker 256 tumors at 24 hr after i.v. injection suggests that tumor doubling time may not significantly effect the uptake of radioactivity.

The levels of NM-324 retention in the kidney and liver of the Lewis rat model and the Sprague Dawley-Walker model are different. At 24 hr after injection, the RMT-bearing Lewis rats had radioactivity levels of 4.55 and 2.89 %ID/g for kidney and liver, respectively, which is twice that found in previous studies with Walker tumor-bearing Sprague Dawley rats (16). The strain difference in the biodistribution of NM-324 cannot be explained at this time.

In the rat mammary tumor model, tumor-to-normal tissue ratios reached a maximum at 96 hr with a tumor-to-blood ratio of 8.62 and a tumor-to-muscle ratio of 20.13. This finding is consistent with previous results with other tumor models and shows that the washout of radioactivity from the nontarget tissues is faster than from the tumor (28).

Gamma camera scintigrams of the RMT-bearing Lewis rat afforded visualization of the tumor as early as 1 hr after administration. Since animals were not pretreated with Lugol's solution, activity could be seen in the thyroid at later time points and was attributed to in vivo deiodination of the tracer. Previous biodistribution studies have demonstrated that prior administration of Lugol's solution blocks thyroid uptake of radioactivity in Sprague Dawley rats.

Previous work has shown that NM-324 is excreted from Sprague Dawley rats primarily via urinary excretion (28). Lipid extraction of liver and tumors from the RMT model showed the presence of only parent compound at all time points. This finding was consistent with previous work which indicated that radioactivity found in tissues such as blood, liver and tumor was composed of intact NM-324 (16).

Parallel studies performed in athymic nude mice with the estrogen-independent HT-39 tumor showed that uptake of radioactivity by the tumor reaches a maximum of 4.96 %ID/g at 48 hr. Radioactivity levels were also high at early time points in

normal tissues such as kidney, liver and duodenum. However, at 196 hr after i.v. administration, tumor-nontarget tissue ratios were all greater than one, indicating that clearance from the tumor was much slower than that of normal organs. At this time, the tumor-to-blood ratio was 16.9 and the tumor-to-muscle ratio was 19.1. These results are similar to those found previously in nude mice bearing ovarian, small cell carcinoma, or melanoma human tumor xenografts (16).

Lipid extraction of liver and tumor taken from athymic mice at 48 hr and 196 hr revealed the presence of only intact ^{125}I-NM-324. Moreover, gamma camera scintigraphy showed a pattern of uptake and clearance which is very similar to that of RMT rats. However, uptake in the tumor required a much longer time to reach a maximum in the mouse model and the abdominal area contained large quantities of radioactivity, primarily associated with liver, kidney and the GI tract.

The overall uptake, retention and clearance of NM-324 in the two breast tumor models followed a similar trend. As seen in Figures 2 and 3, the relationship between the radioactivity levels in the blood, lung or muscle, and the tumor were similar. The tissue uptake of NM-324, however was much greater in athymic mice than in the rat in all tissues as demonstrated by a maximal HT-39 tumor uptake of 4.96 %ID/g compared to a maximal uptake in the RMT model of 1.65%.

CONCLUSION

This study sought to examine the potential of a radioiodinated phospholipid ether analog (NM-324) as a breast tumor imaging agent. Uptake and retention of the probe was demonstrated in a rat mammary tumor and in human breast tumor xenografts in athymic mice. In addition to tumors, kidneys, liver and duodenum were competing organs for retention of the tracer. From a clinical standpoint, it is encouraging to be able to readily visualize the rat mammary tumor by external scanning as early as 1 hr after administration of NM-324. Clearly, more studies remain to be performed on NM-324 as well as closely related analogs to ascertain their varying capacities to accumulate in tumors versus normal tissue. The preliminary patient studies now in progress with ^{131}I-NM-324 will help to correlate human pharmacokinetics with those observed in studies with various animal models. If the pharmacokinetics of NM-324 in humans is acceptable, further studies will be undertaken to evaluate the efficacy of this type of agent for imaging breast and other nonabdominal tumors.

REFERENCES

1. Goldenberg DM, Larson SM. Radioimmunodetection in cancer identification. *J Nucl Med* 1992;33:803–814.
2. Thor AD, Edgerton SM. Monoclonal antibodies reactive with human breast and ovarian carcinoma: in vivo applications. *Semin Nucl Med* 1989;19:295–308.
3. DeNardo SJ, O'Grady LF, Macey DJ, et al. Quantitative imaging of mouse L-6 monoclonal antibody in breast cancer patients to develop a therapeutic strategy. *Nucl Med Biol* 1991;18:621–631.
4. Ribeiro-Barra MJ, Foulon C, Baulieu JL, et al. Estrogen receptor imaging with 17α-[^{123}I]iodovinyl-11β methoxyestradiol (MIVE$_2$)—part II. Preliminary results in patients with breast carcinoma. *Nucl Med Biol* 1992;19:263–267.
5. Mintun MA, Welch MJ, Siegel BA, et al. Breast cancer: PET imaging of estrogen receptors. *Radiology* 1988;169:45–48.
6. Furr BJA, Jordan VC. The pharmacology and clinical uses of tamoxifen. *Pharmacol Ther* 1984;25:127–132.
7. Pomper MG, Pinney KG, Carlson KE, et al. Target tissue uptake selectivity of three fluorine-substituted progestins: potential imaging agents for receptor positive breast tumors. *Nucl Med Biol* 1990;17:309–319.
8. Wahl RL, Cody R, Hutchins G, Kuhl D. 2-Deoxy-2-F-18-fluoro-glucose (FDG) PET assessment of the early metabolic response of breast carcinoma to chemochrono-therapy [Abstract]. *Proc Am Assoc Cancer Res* 1990;31:A1088.

9. Cody R, Hutchins G, Wahl RL. PET imaging of primary and metastatic breast cancer with 2-fluoro-18F-2-deoxy-d-glucose (FDG) [Abstract]. *Proc Am Soc Clin Oncol* 1990;9:A189.
10. Paul R, Parviainen S. Dynamic [^{18}F]-2-fluoro-2-deoxy-D-glucose (FDG) scintigraphy of normal and tumor-bearing rats. *Res Exp Med (Berl)* 1986;186(4):249–258.
11. Snyder F, Wood R. Alkyl and alk-1-enyl ethers of glycerol in lipids from normal and neoplastic human tissues. *Cancer Res* 1969;29:251–257.
12. Snyder F, Blank ML, Morris HP. Occurrence and nature of O-alkyl and O-alk-1-enyl moieties of glycerol in lipids of Morris transplanted hepatomas and normal rat livers. *Biochim Biophys Acta* 1969;176:502–510.
13. Soodsma JF, Piantadosi C, Snyder F. The biocleavage of alkyl glyceryl ethers in Morris hepatomas and other transplantable neoplasms. *Cancer Res* 1970;30:309–311.
14. Meyer KL, Schwendner SW, Counsell RE. Potential tumor or organ imaging agents 30. Radioiodinated phospholipid ethers. *J Med Chem* 1989;32:2142–2147.
15. Counsell RE, Schwendner SW, Meyer KL, Haradahira T, Gross MD. Tumor visualization with a radioiodinated phospholipid ether. *J Nucl Med* 1990;31:332–336.
16. Plotzke KP, Haradahira T, Stancato L, et al. Selective localization of radioiodinated alkylphosphocholine derivatives in tumors. *Nucl Med Biol* 1992;19:775–782.
17. Plotzke KP, Fisher SJ, Wahl RL, Olken NM, Skinner S, Gross MD, Counsell RE. Selective localization of a radioiodinated phospholipid ether analog in human tumor xenografts. *J Nucl Med* 1993;34:787–792.
18. Ethier SP. Primary culture and serial passage of normal and carcinogen-treated rat mammary epithelial cells in vitro. *J Natl Cancer Inst* 1985;74:1307–1318.
19. Ethier SP, Cundiff KC. Importance of extended growth potential and growth factor independence on in vivo neoplastic potential of primary rat mammary carcinoma cells. *Cancer Res* 1987;47:5316–5322.
20. Ethier SP, Moorthy R. Multiple growth factor independence in rat mammary carcinoma cells. *Breast Cancer Res Treat* 1991;18:73–81.
21. Simpson RU, Arnold AJ. Calcium antagonizes 1,25-dihydroxyvitamin D3 inhibition of breast cancer cell proliferation. *Endocrinology* 1986;119:2284–2289.
22. Simpson RU, Taylor JT. Regulation of cancer cell proliferation by calcium antagonists. *Exper Oncol (Life Sci Adv)* 1988;7:81–89.
23. Taylor JT, Simpson RU. Inhibition of cancer cell growth by calcium channel antagonists in the athymic mouse. *Cancer Res* 1992;52:2413–2418.
24. Weichert JP, VanDort ME, Groziak MP, Counsell RE. Radioiodination via isotope exchange in pivalic acid. *Appl Radiat Isot* 1986;37:907–913.
25. Folch J, Lees M, Sloane-Stanley FG. A simple method for the isolation of total lipids from animal tissues. *J Biol Chem* 1957;226:497–509.
26. Brown RS, Leung JY, Fisher SJ, Frey KA, Ethier SP, Wahl RL. Intratumoral distribution of tritiated fluorodeoxyglucose in breast carcinoma: I. Are inflammatory cells important? *J Nucl Med* 1995;36:1854–1861.
27. Brown RS, Fisher SJ, Wahl RL. Autoradiographic evaluation of the intratumoral distribution of 2-deoxy-D-glucose and monoclonal antibodies in xenografts of human ovarian adenocarcinoma. *J Nucl Med* 1993;34:75–82.
28. Plotzke KP, Rampy MA, Meyer K, et al. Biodistribution, metabolism, and excretion of radioiodinated phospholipid ether analogs in tumor-bearing rats. *J Nucl Biol Med* 1993;37:264–272.

Intraperitoneal Indium-111- and Yttrium-90-Labeled Human IgM (AC6C3-2B12) in Nude Mice Bearing Peritoneal Carcinomatosis

Syed M. Quadri, Atif B. Malik, Hung B. Chu, Ralph S. Freedman and Huibert M. Vriesendorp

Departments of Experimental Radiotherapy and Gynecological Oncology, University of Texas M.D. Anderson Cancer Center, Houston, Texas

Radiolabeled monoclonal antibodies are utilized increasingly for the diagnosis and treatment of human cancer. Tumor targeting of radiolabeled human monoclonal IgM improves with compartmental administration and might be useful for the diagnosis or treatment of peritoneal carcinomatosis. **Methods:** A human monoclonal antibody IgMλ (AC6C3-B12) reactive with human adenocarcinomas was conjugated to isothiocyanato-2-benzyl-3-methyl-diethylenetri-amine-penta-acetic acid and labeled with either ^{111}In or ^{90}Y. Nude mice bearing intra-abdominal lumps of a human colorectal carci-noma cell line (SW620) were used as a model for peritoneal carcinomatosis. A human monoclonal antibody IgMλ (CR4E8) reac-tive with human squamous-cell carcinoma was used as a control. **Results:** Indium-111-IgM and ^{90}Y-IgM immunoconjugates were compared in nude mice at 2, 24, 72, 120 and 144 hr after intraperito-neal administration. Both showed high specific tumor uptake. The tumor-effective half-lives of the immunoconjugates were 39 hr for indium and 46 hr for yttrium. Tumor-to-normal organ ratios were high and similar for both reagents. Only the femur uptake at later time points was relatively higher for the ^{90}Y-IgM than for ^{111}In-IgM. The tumor uptake of specific AC6C3-2B12 was about fourfold higher than the uptake of aspecific CR4E8 at 24 and 120 hr. **Conclusion:** The combination of ^{111}In- and ^{90}Y-labeled AC6C3-2B12 offers a new opportunity to develop safer and more effective methods for diagnos-ing and treating human patients with peritoneal carcinomatosis.

Key Words: indium-111; yttrium-90; human IgM; biodistribution; intraperitoneal administration

A radiolabeled immunoglobulin therapy (RIT) strategy can be applied rationally and safely if results of a diagnostic radioim-munoconjugate are predictive for results of a therapeutic radio-immunoconjugate. First, patients receive an immunoconjugate reactive with tumor-associated antigens as a diagnostic reagent labeled with a gamma-emitting isotope. If immunoscintigraphy studies with a gamma camera show that the radioimmunocon-jugate behaves satisfactorily in vivo, the same immunoconju-gate can be administered again, now labeled with a beta-emitting isotope, for treatment. The diagnostic study with a gamma-emitting reagent can be performed in an outpatient setting because the total administered activity is low. Subse-quent therapy with beta-emitting isotope can also be accom-plished on an outpatient basis because most of the beta-emission energy is absorbed in vivo within a few millimeters of the radioimmunoconjugate.

Previous experience in preclinical and clinical RIT has shown that under the proper conditions, the administration of ^{111}In-labeled immunoconjugate before the introduction of the same immunoconjugate labeled with ^{90}Y can be useful in predicting tumor targeting and tumor dosimetry before therapy (*1–10*). The physical characteristics of ^{111}In and ^{90}Y are well-suited for the diagnosis and treatment of cancer, respectively. Both radiometals require a bifunctional chelating agent for stable binding to an immunoglobulin. The coordination chemistries of ^{90}Y and ^{111}In are similar but not identical; therefore, the combined use of indium- and yttrium-labeled immunoconju-gates requires prior verification and correlation of their in vivo pharmacokinetic characteristics, such as chelation stability, tumor uptake and biodistribution.

Two problems have impeded the broader application of RIT in patients: low uptake of radioimmunoconjugate in tumors